Biochimica et Biophysica Acta 1837 (2014) 1964–1972

Contents lists available at ScienceDirect

Biochimica et Biophysica Acta

journal homepage: www.elsevier.com/locate/bbabio

Electrostatic interactions and hydrogen bond dynamics in chloride pumping by halorhodopsin

Eduardo Jardón-Valadez [a], Ana-Nicoleta Bondar [b,*], Douglas J. Tobias [c]

[a] Departamento de Recursos de la Tierra, Universidad Autónoma Metropolitana-Lerma, Lerma de Villada, Estado de México 52005, México
[b] Theoretical Molecular Biophysics Department of Physics, Freie University Arnimallee 14, Berlin 14195, Germany
[c] Department of Chemistry, University of California, Irvine, CA 92697–2025, USA

ARTICLE INFO

Article history:
Received 14 July 2014
Received in revised form 15 September 2014
Accepted 17 September 2014
Available online 23 September 2014

Keywords:
Chloride transport
Protein dynamics
Electrostatic interactions
Inter-helical hydrogen bonding
Intra-helical hydrogen bonding

ABSTRACT

Translocation of negatively charged ions across cell membranes by ion pumps raises the question as to how protein interactions control the location and dynamics of the ion. Here we address this question by performing extensive molecular dynamics simulations of wild type and mutant halorhodopsin, a seven-helical transmembrane protein that translocates chloride ions upon light absorption. We find that inter-helical hydrogen bonds mediated by a key arginine group largely govern the dynamics of the protein and water groups coordinating the chloride ion.

1. Introduction

Ion pumps are membrane proteins that translocate ions against their electrochemical gradient. The mechanism by which the protein and water dynamics couple to fluctuations in the location of the ions inside the pump is an open question. Here we address this question by using as a model system halorhodopsin (HR), a light-driven pump that translocates chloride ions from the extracellular to the cytoplasmic side of the plasma membrane in archaea [1]. Ion translocation by halorhodopsins is essential for maintaining the membrane bioenergetics in archaea [2], and is now being exploited to help control the transmembrane potential of neurons in optogenetics applications [3]. To understand how the protein controls movement of the ion, we dissected the coupling between the dynamics of a chloride ion bound to the protein and protein hydrogen bonding.

Knowledge on chloride ion translocation by HR comes largely from studies on the *Natronomonas pharaonis* halorhodopsin (pHR) or *Halobacterium salinarium* halorhodopsin (sHR). In both halorhodopsins, absorption of light by the covalently bound retinal chromophore triggers a reaction cycle during which the protein passes through a sequence of intermediate states, HR → K → L1 → L2 → N → O → HR′ [4], of which the last two steps are associated with, respectively, the release and uptake of a chloride ion [5,6].

Crystal structures suggest that in the pHR resting state there is a chloride ion tightly bound inside the protein, where it interacts with the retinal Schiff base, R123, T126, S130 and D252 (site-1 in Fig. 1E). A second chloride ion is located on the cytoplasmic side of the pump, where it is coordinated by side chains of two different protomers within the trimer (site-2 in Fig. 1C). Diffraction data collected after a post-crystallization treatment, in which pHR crystals were soaked in a sodium bromide solution, suggest the existence of a third binding site, site-3, at the extracellular side between loops BC and FG [7]. A hydrophobic segment between helices B and C (Fig. 1E) is thought to help prevent a rapid chloride exchange between site-1 and the extracellular side [8].

The structural features of pHR summarized above are very similar to those observed for sHR [9]. Understanding sHR is somewhat complicated by the observation that it shows light–dark adaptation, a process which leads to the protein existing as a mixture of both all-*trans* and 13-*cis, 15-syn* retinal isomeric states [10]. Since pHR does not undergo dark adaptation [11], it is a more convenient model system to study ion translocation, and hence we used pHR in our work. In what follows, all amino acid residue numbers refer to the pHR sequence and protein structure, unless otherwise specified.

The movement of the chloride ion across the pump is thought to occur in four discrete steps. In the all-*trans* resting state HR and the first two 13-*cis* states, K and L1, the chloride ion appears to remain largely in the same location as in the starting HR state [12–14]. Nevertheless, perturbed interactions of the Schiff base and R123 may weaken

* Corresponding author.
E-mail address: nbondar@zedat.fu-berlin.de (A.-N. Bondar).

http://dx.doi.org/10.1016/j.bbabio.2014.09.006
0005-2728/

Table 1
Summary of experimental observations from site-directed mutagenesis of *Natromonas pharaonis* halorhodopsin.

Mutant	Location	Observations	Ref.
H100A	BC loop	Low conducting rates and decreased chloride binding.	[49]
E234D	FG loop	Changes in FTIR bands upon formation of L2.	[50]
R123K R123Q R123H	Helix C	R123H and R123Q abolish ion conduction; R123K decreases the binding affinity relative to the wild type.	[18]
S130A S130T S130C	Helix C	The dissociation constants increase from 5 mM in the wild type to 89, 153 and 159 mM for mutants S130A, S130T and S130C, respectively.	[51]
T126V	Helix C	Slower rise of the N intermediate state than in the wild type.	[15]

All amino acid residues from Table 1 are depicted in Fig. 1E.

the chloride interactions at site-1, and set the stage for the chloride displacement from site-1 to the cytoplasmic side of the retinal in the L2 intermediate state [15]. On the cytoplasmic side, the chloride ion binds to K215 and T218 on helix F [15]. Structural information about the N and O intermediates is scarce, and different HR variants may have different kinetics of these states; for example, the O state is undetectable in sHR [10], whereas an O-like crystal structure could be obtained for pHR [7]. Release of the chloride ion to the cytoplasm involves outward motion of helix F, as observed during translocation of azide anions [16]. Opening of the cytoplasmic channel allows water molecules to hydrate the chloride ion, replacing chloride–protein interactions with chloride–water interactions. Movement of helix F back to its original location occurs during the decay of O into HR′; a chloride ion is loaded at site-1, and the translocation cycle can restart [15].

The highly conserved helix-C amino acid residue R123 is essential for the translocation of ions across HR [17]. In the HR resting state R123 hydrogen bonds to groups on helices A and G (Fig. 1E). The importance of R123 for HR function is highlighted by its conservation in all microbial-type rhodopsins [17], and by site-directed mutagenesis experiments indicating that the R123Q and R123H mutations abolish ion translocation [18]. The observation that even the conservative mutation R123K increases significantly the dissociation constant [18] suggests that not only the positive charge, but also the hydrogen bonding pattern is important for controlling the location of the chloride ion. To understand how R123 helps control chloride binding and translocation by halorhodopsins, we performed extensive all-atom molecular dynamics simulations on wild-type and three R123 mutants of pHR. We find that R123 provides an attractive electric potential at site-1 for binding anions and mediates a dynamical interhelical hydrogen-bonded network that couples protein conformational dynamics to the dynamics of the chloride ion in site-1.

2. Methods

2.1. Protein structure

For the starting protein coordinates we used the crystal structure of wild-type HR (Fig. 1A) from *Natronomonas pharaonis* (PDB:3A7K [8]). The crystal structure includes coordinates for the protein trimer, the covalently-attached retinal chromophore, three carotenoid lipid molecules (bacterioruberin), 144 water molecules, two chloride ions per protein monomer, and lipid fragments in the intra-trimer space, which were modeled as palmitoyl-oleoyl-phosphatidylcholine (POPC) molecules. The protein trimer was oriented with its principal axes along the coordinate axes, and then embedded in a hydrated lipid membrane consisting of 515 POPC lipids and 32,700 water molecules. Sodium ions were added for charge neutrality. The simulation system consisted of approximately 180,000 atoms. The R123A, R123L, and R123K mutants were modeled using PSFGEN and CHARMM softwares [19,20].

2.2. Potential energy function

The CHARMM22 and CHARMM36 force fields [21,22] were used for protein and lipids, respectively, and the TIP3P model was used for the water molecules [23]. Polyene chains (retinal and bacterioruberin) were modeled using a parameter set optimized for retinal in the gas phase [24] together with the partial charges calculated by Nina et al. [25].

2.3. Molecular dynamics simulations

The molecular dynamics simulations were performed using the following protocol. First, the simulation system was geometry optimized by performing 10,000 steps of conjugate-gradient energy minimization. During the geometry optimization we fixed the chloride ions, the protein and the bacterioruberin heavy atoms, as well as lipid and water molecules resolved in the crystal structure. The equilibration was performed by gradual releasing of harmonic positional constraints, starting with a force constant of 25 kcal/mol · Å, which was reduced to 15, 10, 5, 2, and 1 kcal/mol · Å in a series of MD simulations, each of which was carried out for 200 ps. The simulation was subsequently continued without any restraints for 100 ns at a constant pressure of 1 bar and a constant temperature of 310 K in the NPT ensemble. The MD simulations were run with the NAMD 2.8 software package [26]. A reversible multiple time step algorithm [27] was used to integrate the equations of motion with time steps of 1 fs for bonded forces, 2 fs for short-range, non-bonded forces, and 4 fs for long-range electrostatic forces. The smooth particle mesh Ewald (PME) method [28,29] was used to calculate electrostatic interactions. The short-range interactions were cut off at 12 Å. All bond lengths involving hydrogen atoms were held fixed using the SHAKE [30] and SETTLE [31] algorithms. A Langevin dynamics scheme was used for thermostatting. Nosé–Hoover–Langevin pistons were used for pressure control [32,33]. Molecular graphics and simulation analyses were generated with the VMD 1.8.7 software package [34]. Sequence alignments were generated by using Modeller version 9.11 [35,36], and reading the amino acid sequence directly from the PDB files. All amino acid numbering used here corresponds to the pHR sequence.

2.4. Computation of the isopotential surfaces

To illustrate the electrostatic potential experienced by the chloride ion at site-1, we used the protocol below to calculate the electrostatic potential by considering the site-1 chloride ion as a ghost particle — that is, for each monomer, we calculated isosurfaces for the electric potential in the interhelical region by considering only the protein atoms and water molecules within 20 Å of the chloride ion, under the assumption that the contribution from the lipids is similar in each system and, hence, can be ignored because we are primarily interested in differences between the wild-type and mutant proteins.

To compute the electrostatic potential maps we used the PME volume map plugin of the VMD package [34]. This involved solving the Poisson equation for a discretized charge density in a 192 × 192 × 120 mesh, at 0.2 Å resolution, based on coordinate sets taken each 100 ps from the last 10 ns of each simulation [37]. To visualize the electrostatic potential maps, and ease the comparison between different simulations, we superposed onto the map the coordinates of the protein and site-1 ion from the starting coordinate snapshot.

3. Results

3.1. Wild type halorhodopsin in a hydrated lipid bilayer

We find that simulations of the pHR trimer embedded in the lipid bilayer at room temperature preserve well the overall structure of the protein. The backbone root-mean-squared deviations (RMSD) relative

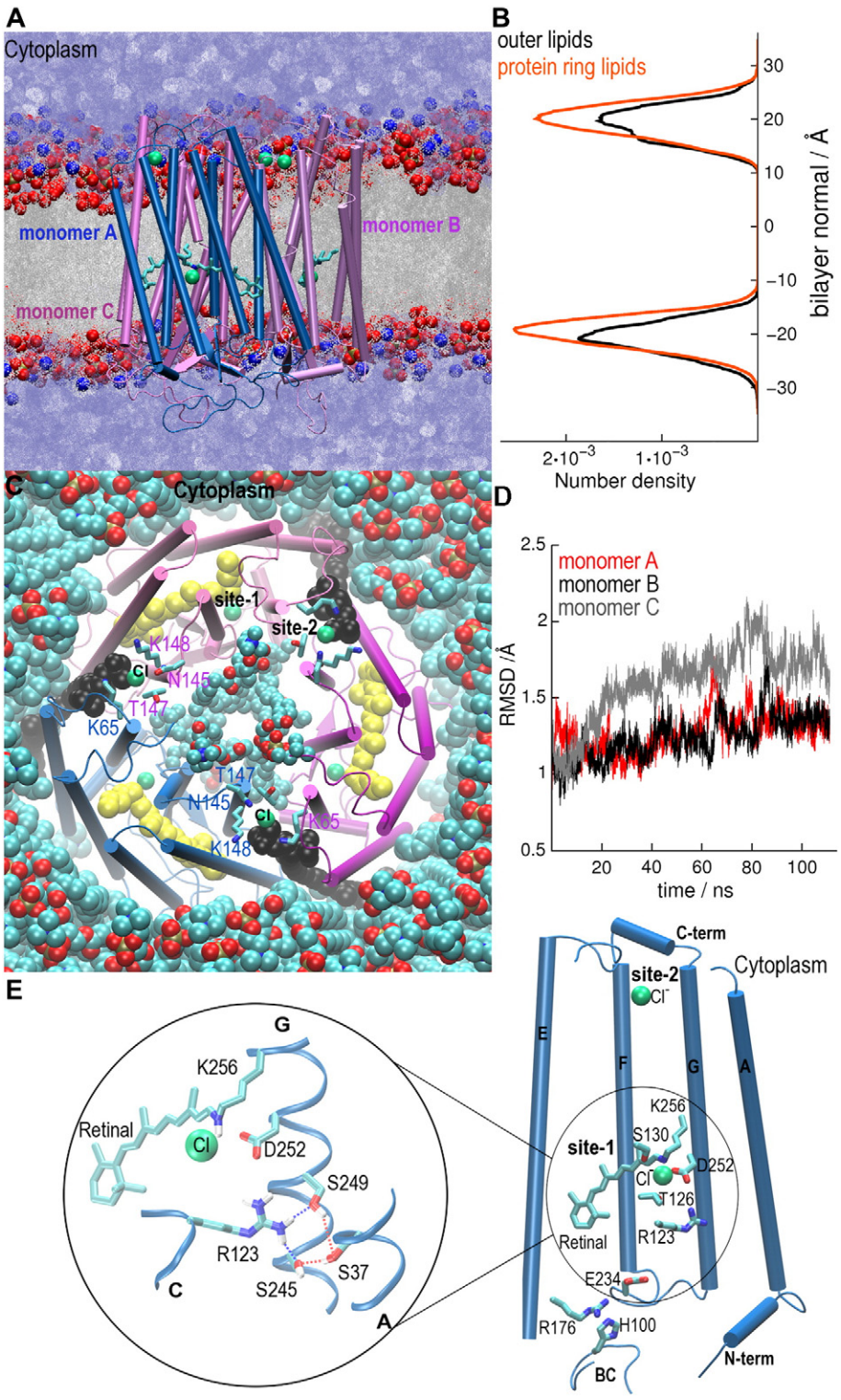

Fig. 1. The *Natronomonas pharaonis* halorhodopsin (pRH) trimer in a hydrated lipid membrane patch. (A) Monomers A, B, and C depicted as cartoons are colored blue, mauve, and pink, respectively. Chloride ions are shown as green spheres, lipid oxygen atoms are in red, nitrogen in blue, and phosphate atoms are in orange. Lipid tails are depicted as gray bonds. The retinal molecules and K256 sidechains are shown as bonds with the carbon atoms in cyan. Hydrogen atoms are not shown. (B) Thickness of the lipid bilayer close to the protein and at remote distances. The thickness of the lipid bilayer is estimated from the number density of the lipid phosphorous atoms, computed for lipids within 15 Å of the protein, and for lipids further away from the protein. Each number density is normalized to the number of lipids in the corresponding region. (C) View from the cytoplasmic side of the simulation box. Bacterioruberin is shown as black van der Waals spheres, chloride ions are in green at site-1 and site-2, and retinal with K256 are depicted as yellow van der Waals spheres. Lipid molecules are depicted as van der Waals spheres with carbon atoms in cyan, oxygen — red, nitrogen — blue, and phosphorous atoms in orange. Specific sidechains are depicted using the same color code. (D) Root-mean-squared deviation (RMSD, in Å) of the backbone heavy atoms in the simulation of wild-type halorhodopsin, calculated relative to the starting crystal structure. (E) Close-up view of site-1 in the crystal structure [8] illustrating hydrogen bonding of R123.

to the crystal structure calculated for each monomer converge to values of less than 2 Å (Fig. 1D). To compare the protein conformation in the three monomers A, B and C we computed positional RMSD matrices from the trajectory of wild-type halorhodopsin (and mutants; Fig. S1);

except for the BC loop (T90 to T119) in monomer C, all RMSD values were within 2.5 Å.

To evaluate any long distance correlations between protein groups we calculated the covariance matrix for the Cα atoms of each monomer by collecting frames every 100 ps along the second half of the simulation trajectories (Fig. S2). In all simulations there are correlations along the diagonal matrix, which represent the motion of the backbone atoms.

The lipid bilayer around the protein was not perturbed significantly, with a bilayer thickness close to that at remote distances from the protein (Fig. 1B). Lipids fill the central cavity of the trimer crystal structure, and the bacterioruberin molecules remain in contact with protein monomers and lipid bilayer atoms (Figs. 1C, S3).

Water molecules were stable in cavities within the interhelical region, for instance, the one delineated by helices C, D and F of monomer A (Fig. 2A). Water molecules in the inter-helical region of pHR play a functional role, as suggested by changes in the dynamics of water molecules detected by time-resolved FTIR experiments for the productive pumping intermediates [38]. In our simulations, water molecules resolved in the crystal structure (Fig. 2B) remain in the interhelical region, while those at the interfaces moved to the bulk solution. A few bulk water molecules entered the interhelical region (Fig. S4). As a result of the water dynamics, in each pHR monomer there are on average one–two water molecules at site-1 (i.e., in the middle of the protein, Fig. 2A–C); there are more water molecules in the extracellular than in the cytoplasmic half of the protein.

Chloride ions initially bound at site-2 (Fig. 1C) moved into the aqueous medium within the first ns of trajectory. In contrast, the chloride ion at site-1 remains close to its location in the starting crystal structure (Figs. 2A, S4). We monitored the coordinate along the membrane normal (z coordinate) of the chloride ion at site-1 relative to its initial position in the crystal structure. With this measure, a positive value means that the ion moves towards the cytoplasmic side. In the wild-type protein, the chloride ion at site-1 sampled a well confined space in the interval $1.3\ \text{Å} > z > -3\ \text{Å}$ (Fig. S5).

3.2. General structural features of the mutant proteins

On the timescale of our simulations, the effects of the R123 mutation are mostly local. The positional RMSD matrices that compare each mutant protein monomer to the wild-type monomer (Fig. S1) indicate small values within 2.5 Å, with slightly larger deviations for the flexible BC loop. The secondary structure is well preserved (Fig. S6). In some α-helical segments we detected transient turns — for example, in helix C around L129, and in helix F around I227. The BC loop undergoes transitions between β-sheets and bends, and between bends and turns; these transitions are fast, occurring on the ~100 ps time scale.

The dihedral angles along the retinal polyene chain in mutant proteins remain relatively close to the wild-type halorhodopsin (Supplementary Table ST1). The covariance matrices of the Cα atoms indicate that the mutants show only minor variations in backbone fluctuations relative to the wild type (Fig. S2). Therefore, in what follows we concentrate on the local changes in chloride, water and protein dynamics caused by mutating R123.

3.3. Electrostatic interactions at site-1

To illustrate the electrostatic interactions at site-1, we used the last 10 ns of each simulation to compute the PME map [37] for the protein atoms and the internal water molecules, and superposed the map onto the initial coordinate snapshot from each simulation (Fig. 3; see the Methods section). To identify the volume sampled by the chloride ion at site-1, computation of the isodensity surfaces revealed its average location during the last 10 ns of each simulation (Fig. S4).

We find that, in the wild-type protein, the chloride ion experiences an attractive potential at the isovalue of 15 kT/e (Fig. 3). Away from site-1, the isopotential values switched to anion repulsive values. The

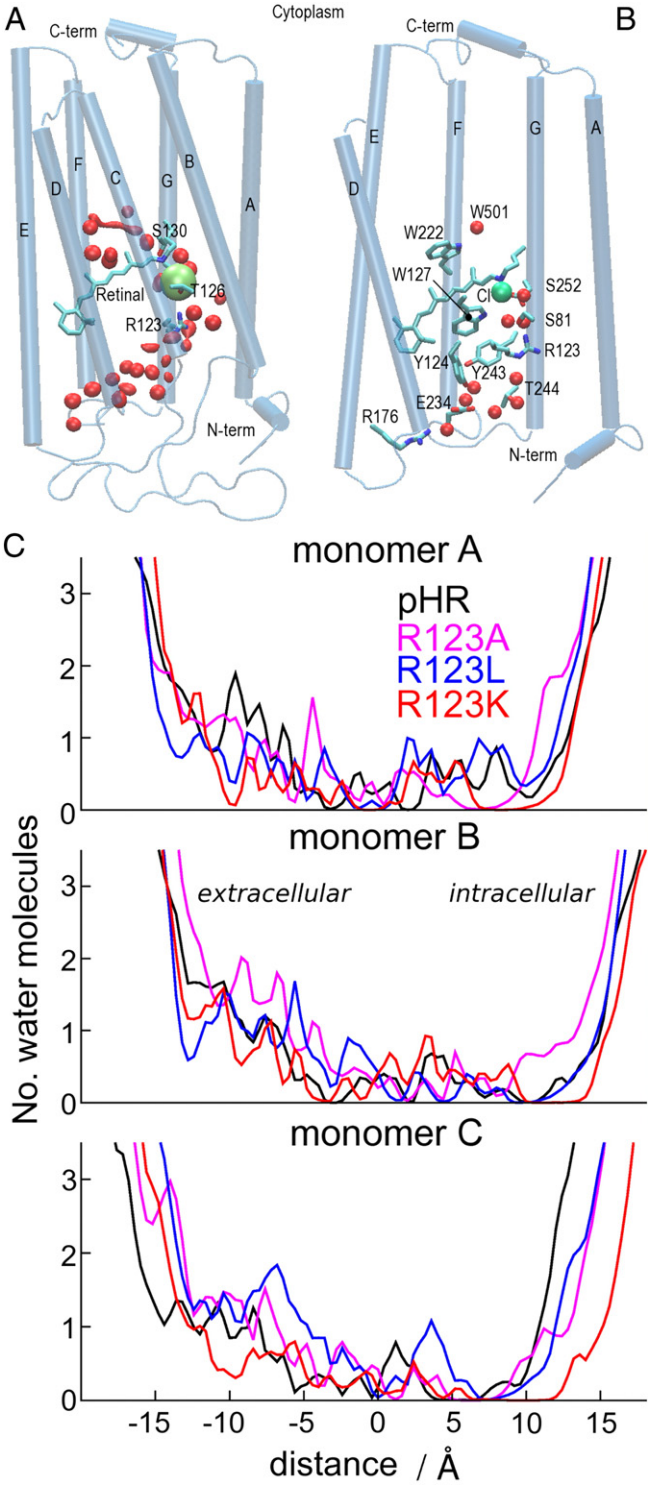

Fig. 2. Dynamics of the chloride ion and water molecules in the interhelical region. (A) Isodensity distributions for the chloride ion and the internal water molecules colored, respectively, as green and red surfaces. Surfaces correspond to the average number density over the last 20 ns. Water and Cl^- isodensity values were set to 1 and 0.1 molecules/Å^3 or ions/Å^3, respectively. The grid resolution was set at 0.2 Å and the molecule/ion distribution in the grid points was weighted by the atomic mass. (B) Internal water molecules in the crystal structure of halorhodopsin [8]. (C) Number of water molecules in the interhelical region, along the bilayer normal, for the last 20 ns of the trajectory.

PME map computed for the R123K mutant displayed a similar profile, with positive values at site-1 (Fig. 3). In contrast, the site-1 isovalues for R123A and R123L became negative (Fig. 3). That is, a positively-charged sidechain, R123 or K123, is needed to provide the chloride ion

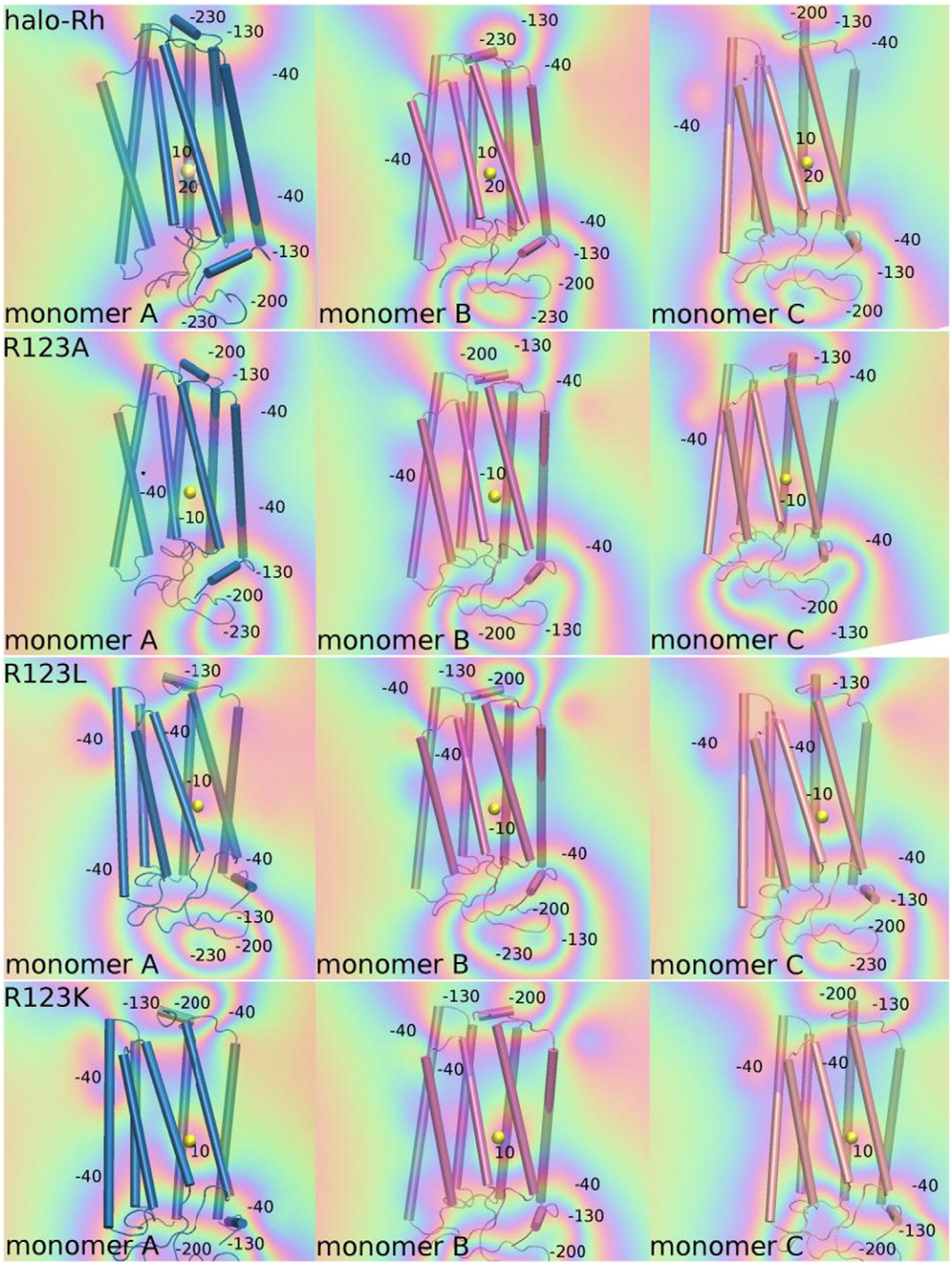

Fig. 3. The positively-charged sidechain R/K123 provides a favorable electrostatic environment for the chloride ion at site-1. The panels depict the contours of the electrostatic potential (in *kT*/*e* units at 300 K) for a discretized charge distribution in a grid of 0.2 Å resolution for wild-type and mutant pHR. The computations were performed for each monomer by including only the protein atoms and water molecules within 20 Å of the site-1 chloride ion. The location of the chloride ion in the starting crystal structure is shown as a yellow-sphere. The numbers indicate the values of selected isosurfaces.

with a favorable electrostatic environment. These observations confirm the key role of a basic sidechain at position 123 in stabilizing the chloride ion inside the protein.

3.4. Intra- and inter-helical hydrogen bonding

Inspection of the crystal structure and sequence analyses indicates that halorhodopsins contain conserved Ser/Thr groups along the transmembrane segments (Fig. 4). At the extracellular side, helices A, B, C and G contain multiple Ser and Thr groups: helices A, B, C and G have the conserved motifs $S_{36}S_{37}$, $S_{78}xxS_{81}$, $T_{126}xxxS_{130}$, and $T_{244}SxxxS_{249}$ (Fig. 4B). These motifs are located at functionally important sites of the protein: helix-C T126/S130 and helix-B S78/S81/T83/S87 are located close to site-1, and helix-G S245/S249 forms hydrogen bonds with the side chain of R123 in the crystal structure (Fig. 1E). Helix F has on its cytoplasmic side two side chains with hydroxyl groups, S212 and T218.

The observation of multiple Ser/Thr groups located at functional motifs of the protein is potentially important because Ser/Thr groups can have both intra- and inter-helical hydrogen bonds. By competing with

backbone amide groups for hydrogen bonding to carbonyls, Ser/Thr groups can weaken the regular amide/carbonyl backbone hydrogen bonding, increasing the local dynamics of the helix [39]. Examples of hydroxyl/carbonyl intra-helical hydrogen bonding include the network of hydrogen bonds involving S245 and S249 on the extracellular side (Fig. S10), the transient hydrogen bond between S212 and the K215 carbonyl (Fig. S7), or the intra-helical hydrogen bond between T218 and the L214 carbonyl (Fig. S7). We suggest that the stable hydrogen bonding between T218 and L214 observed in the wild type (Fig. S7) may contribute to helix F being dynamic.

In addition to shaping the local structure and dynamics of the helix, the hydroxyl groups of Ser/Thr can help in coordinating chloride ions as they pass through the protein. Indeed, in the resting state of the wild-type protein T126 is part of site-1 (Fig. 1E), and helix F-T218 is thought to bind the chloride ion later during the translocation cycle [15]. Using Ser/Thr groups to coordinate chloride ions may be a more general feature of chloride transporters: both the ClC Cl^-/H^+ antiporter [40] and the Cys-loop glutamate-gated chloride channel GluCl [41] are rich in Ser/Thr (Fig. S11). In the case of GluCl, the helix lining the ion conducting pore contains an unusually high number of 7 Ser/Thr groups (Fig. S11 B–C).

3.5. Inter-helical hydrogen bonds mediated by R123

In the simulation of the wild-type protein in the membrane environment, helix-C R123 has hydrogen bonding partners helix-B Y82 and helix-G D252 (Fig. 5A, B), as compared to helix-G S245 and S249 in the crystal structure (Figs. 1E, S9). Similar observations that the interactions between the helix-C arginine and the helix-G aspartate are stronger in simulations than in the crystal structure were made in case of the homologous bacteriorhodopsin [17]. These differences between the

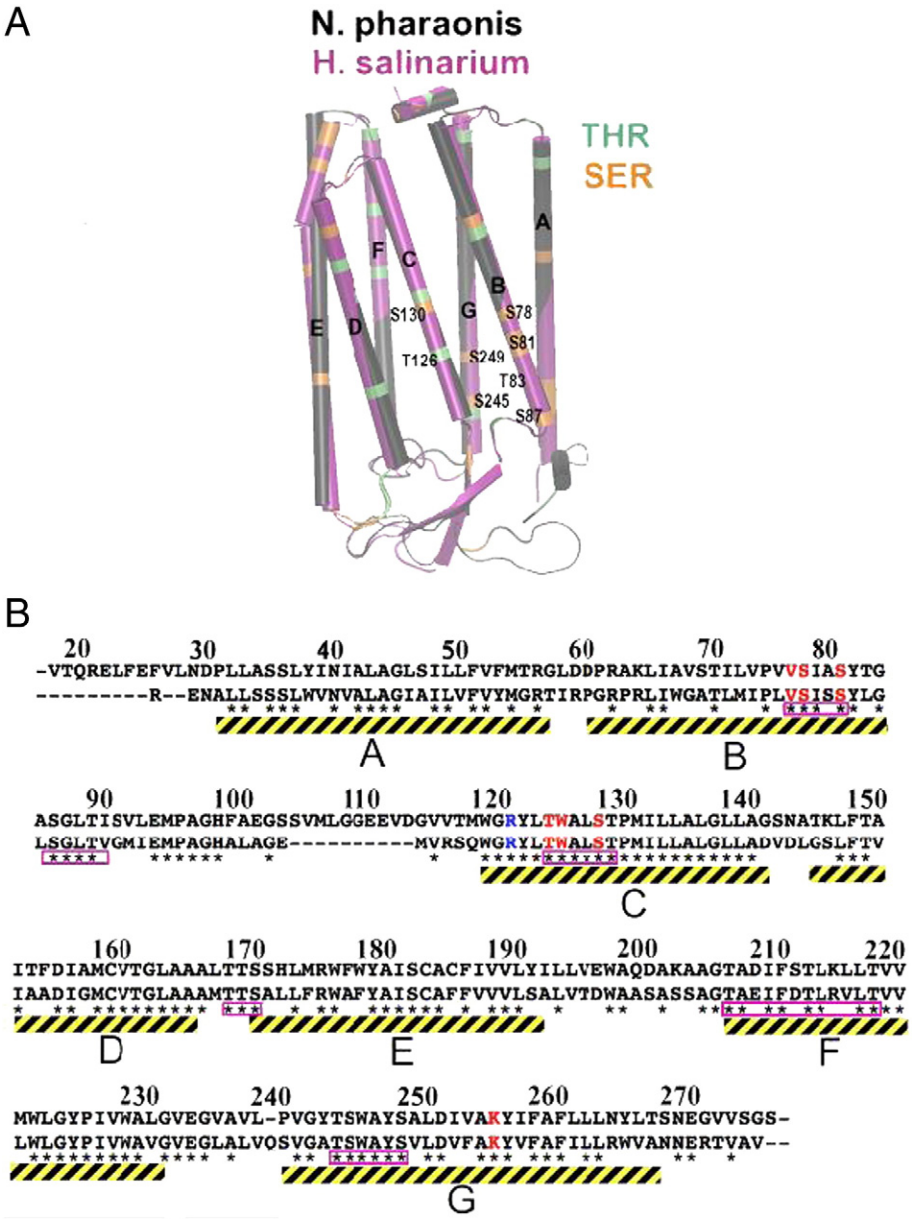

Fig. 4. (A) Structural alignment of *N. pharaonis* (black cartoon) and *H. salinarium* (purple cartoon). Ser and Thr amino acids are highlighted, respectively, as orange and green stripes. Interhelical Ser/Thr motifs are identified at helices B, C, and G along the conducting channel and binding site-1. (B) Sequence alignment of *N. pharaonis* and *H. salinarium*. Numbering corresponds to *N. pharaonis*. Beneath the sequence, bars indicate the transmembrane α-helical domains along the sequences. Asterisks under the sequence alignment identify identical amino acids; 55% identity is found. Ser/Thr motifs are highlighted using magenta rectangles.

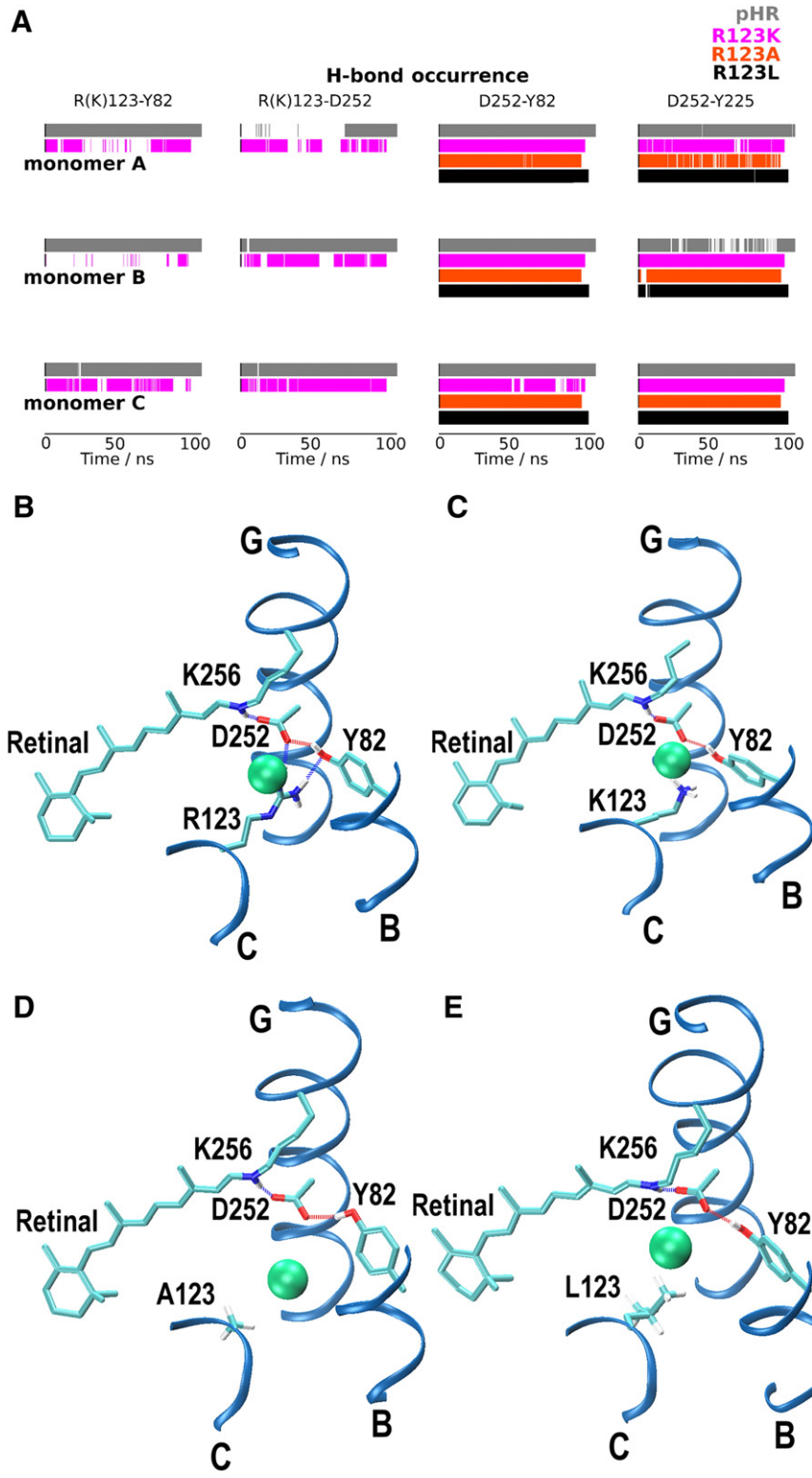

Fig. 5. Inter-helical hydrogen bonding in the wild-type and R123 mutants. (A) Hydrogen-bond occurrence in the wild type and R123 mutants for side chains of residues R(K)123, Y82, D252, and Y225. The time (ns) is shown in the bottom row as the horizontal axis. The lengths of the simulations of wild type, R123A, R123L and R123K mutant halorhodopsin are, respectively, 111 ns, 100 ns, 105 ns, and 102 ns (Table ST2). On the vertical axis, each line represents hydrogen bonding (i.e., distance ≤3.5 Å). The following color coding is used: gray — wild type, magenta — R123K, orange — R123A, and black — R123L. (B–E) Snapshots of the configuration of site-1 of the monomer A in pHR and mutants. The side chains of amino acids Y82, D252, K256, and the retinal are depicted as bonds. For clarity, only fragments of helices C, B, and G are depicted as blue ribbons. The dotted lines indicate hydrogen bonding.

strength of the salt bridge interaction in simulations vs. X-ray crystallography may be due to limitations of the force field, and/or differences in the environment (membrane vs. crystal), and/or to inherent differences in dynamics at room temperature vs. the cryogenic temperatures used in crystallography [17].

3.6. Mutation of R123 perturbs inter-helical hydrogen bonding, water and chloride ion dynamics

In the wild type, hydrogen bonding of R123 with Y82 and of D252 with Y82/Y225 bridges helices B, C, F, and G, and the site-1 chloride

ion has largely stable interactions (Figs. 5A, 6B) with ~4.5 neighbors in its first solvation shell (i.e., within of 3.5 Å, Fig. 6). This coordination number is slightly lower than the value of 5–6 reported in solution [42]. The slightly reduced coordination number of the chloride ion in the pHR binding site-1 relative to solution is due to the protein interactions replacing water within the first solvation shell. In other words, protein interactions are favored in the confined interhelical region.

The hydrogen-bonding network between helices B, C, F, and G is somewhat perturbed in the R123K mutant, in particular the interaction between helix-B Y82 and helix-G D252 (Fig. 5A, C). The coordination number for the chloride ion in R123K remains high as in the wild-type protein (Fig. 6B). However, unlike in the wild-type protein, where the stable protein hydrogen bonding (Fig. 5) appears associated with the chloride coordination number being almost the same (~4.5) in each of the monomers (Fig. 6), in R123K the coordination number is ~3 in monomer C, ~5.5 in monomer B and ~4.5 in monomer B (Fig. 6). These variations in the coordination number computed for R123K suggest that protein, water and chloride interactions are more dynamic in R123K than in the wild type.

In R123A and R123L, since the A/L123 sidechains cannot hydrogen-bond, interactions between helices C and G are broken (Fig. 5A, D, and E). D285 remains hydrogen bonded to Y82/Y225 (Fig. 5A). Absence of hydrogen bonding of helix C to helices B and G is associated with enhanced dynamics of the chloride ion (Figs. 5D–E, S5). The chloride ion from site-1 loses stabilizing first-shell interactions (e.g., with S130, T126, and S81) and as a result it samples a wide region along the membrane normal, up to 6 Å in R123L and 8 Å in R123A (Fig. S5). The displacement of the chloride ion in R123A and R123L is compatible with a role of R123 in preventing leakage of chloride back into the extracellular medium [43].

In summary, all mutations studied here affect the coordination number of the site-1 chloride ion. In R123K the hydrogen bonds between helices B, C and G are perturbed (Fig. 5C) and the tight control of the chloride coordination is lost (Fig. 6). In R123A, the coordination number drops to 2 in monomers A and C, with a water molecule and the sidechains of S81 or T126 as neighbors (Fig. 6). Likewise, the perturbed hydrogen bonds of R123L (Fig. 6) are associated with a lower coordination number of the site-1 chloride ion; the chloride ion is coordinated by 2–3 water molecules and by the side chains of S81, T126, and S130.

3.7. Dynamics of the site-1 chloride ion in the three protein monomers

The monomers of wild-type halorhodopsin have very similar dynamics, including very similar values of the coordination numbers of the chloride ion (Fig. 6), though differences are observed in the dynamics of specific hydrogen bonds — for example, the hydrogen bond between R123 and D252 (Fig. 5A). In contrast, we observe more pronounced differences among the three monomers of the mutant proteins (Fig. 6). The differences in the chloride ion dynamics in the mutant monomers is likely due to insufficient sampling on the hundred nanosecond timescale of our simulations. On the other hand, we note that experiments on some other homotrimeric proteins appear to suggest a complex picture of the conformational dynamics of the monomers [44–46] — for example, the crystal structure of AcrB from Ref. [44] indicates slightly different geometries for each monomer.

4. Conclusions

Hydrogen bonds are essential structural determinants of a membrane protein [47,48]. In the chloride pumping pHR, the highly conserved residue R123 mediates a network of inter-helical hydrogen bonds that help gate access of the chloride ions to the protein (Fig. 1E–F). In the pHR resting state the electrostatic interactions largely favor the presence of a negatively charged chloride ion at site-1 (Figs. 1C, E, 2A, 3). When bound to this site, the chloride ion has 4–5 first-shell neighbors. The dynamics of the chloride ion is exquisitely sensitive to the dynamics of the hydrogen-bonded network mediated by R123. Indeed, the conservative mutation of R123 to Lys, which perturbs hydrogen bonding between helices B, G and G (Figs. 5C & 6), causes loss of the tight control over the interactions of the chloride ion (Fig. 6). In R123A and R123L, lack of hydrogen bonding at position 123 leads to an enhanced dynamics of the chloride ion. The chloride ion samples a wider region within the extracellular half of the protein, and its coordination number decreases to as low as 2 (Fig. 6).

Acknowledgments

A-NB is supported in part by the Marie Curie International Reintegration Award FP7-PEOPLE-2010-RG 276920, and DJT by National Institutes of Health grant P01 GM86685. Computer facilities were

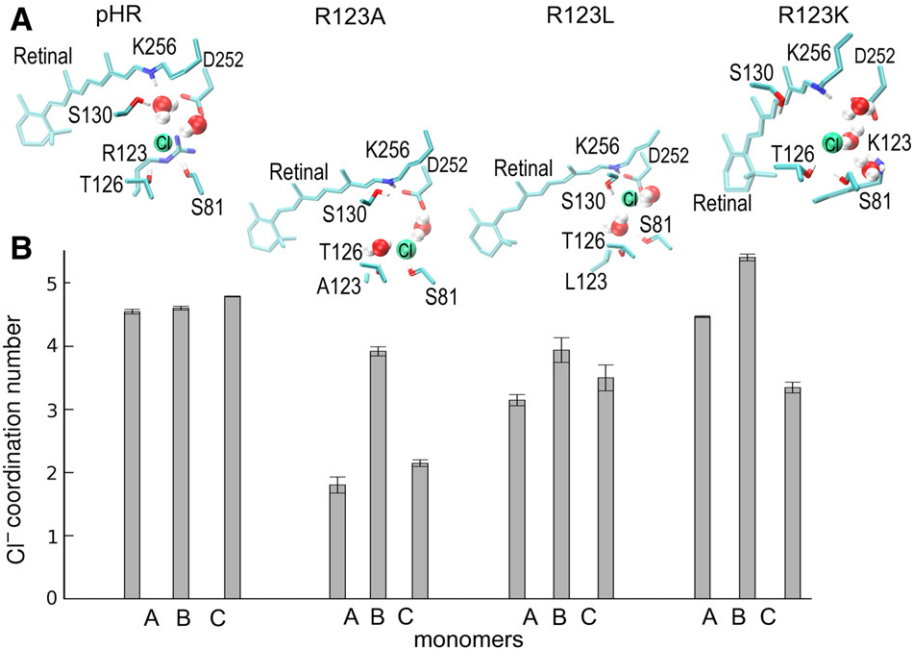

Fig. 6. The coordination number of the site-1 chloride ion is largely affected by mutation of R123. (A) Coordinate snapshots illustrating interactions at site-1 in each of the simulations. (B) Histograms of the number of first shell neighbors of the chloride ion in each monomer.

provided by the University of California-Irvine, Universidad Autónoma Metropolitana-Iztapalapa, and Freie Universität-Berlin. A-NB and EJ-V thank the Center for International Cooperation of the Freie Universität Berlin for supporting a research visit of EJ-V.

Appendix A. Supplementary data

Supplementary data to this article can be found online at http://dx.doi.org/10.1016/j.bbabio.2014.09.006.

References

[1] G. Schaefer, M. Engelhard, V. Müller, Bioenergetics of the Archaea, Microbiol. Mol. Biol. Rev. 63 (1999) 570–619.
[2] R.C.H. del Rosario, E. Mendoza, D. Oesterhelt, Modelling the bioenergetics of *Halobacterium Salinarum* with petri nets, J. Comput. Theor. Nanosci. 6 (2009) 1965–1976.
[3] V. Gradinaru, K.R. Thompson, K. Deisseroth, NpHR: a *Natronomonas halorhodopsin* enhanced for optogenetic applications, Brain Cell Biol. 36 (2008) 129–139.
[4] K. Ludmann, et al., Charge motions during the photocycle of pharaonis halorhodopsin, Biophys. J. 78 (2000) 959–966.
[5] G. Váró, R. Needleman, J.K. Lanyi, Light-driven chloride ion transport by halorhodopsin from *Natronobacterium pharaonis*. 2. Chloride release and uptake, protein conformation change, and thermodynamics, Biochemistry 34 (1995) 14500–14507.
[6] J. Guijarro, M. Engelhard, F. Siebert, Anion uptake in halorhodopsin from *Natromonas pharaonis* studied by FTIR spectroscopy: consequences for the anion transport mechanism, Biochemistry 45 (2006) 11578–11588.
[7] S. Kanada, et al., Crystal structures of an O-like blue form and an anion-free yellow form of pharaonis halorhodopsin, J. Mol. Biol. 413 (2011) 162–176.
[8] T. Kouyama, et al., Crystal structure of the light-driven chloride pump Halorhodopsin from *Natronomonas pharaonis*, J. Mol. Biol. 396 (2010) 564–579.
[9] M. Kolbe, et al., Structure of the light-driven chloride pump halorhodopsin at 1.8 Å resolution, Science 288 (2000) 1390–1396.
[10] G. Váró, et al., Photocycle of halorhodopsin from *Halobacterium salinarium*, Biophys. J. 68 (1995) 2062–2072.
[11] L. Zimányi, J.K. Lanyi, Fourier transform raman study of retinal isomeric composition and equilibration in halorhodopsin, J. Phys. Chem. B 101 (1997) 1930–1933.
[12] C. Pfisterer, A. Gruia, S. Fischer, The mechanism of photo-energy storage in the halorhodopsin chloride pump, J. Biol. Chem. 284 (2009) 13562–13569.
[13] O. Bismuth, et al., Deciphering excited state evolution in halorhodopsin with stimulated emission pumping, J. Phys. Chem. B 114 (2010) 3046–3051.
[14] W. Gmelin, et al., The crystal structure of the L1 intermediate of halorhodopsin at 1.9 angstroms resolution, Photochem. Photobiol. 83 (2006) 369–377.
[15] M. Sato, et al., Role of putative anion-binding sites in cytoplasmic and extracellular channels of *Natronomonas pharaonis* halorhodopsin†, Biochemistry 44 (2005) 4775–4784.
[16] T. Nakanishi, et al., Large deformation of helix f during the photoreaction cycle of Pharaonis Halorhodopsin in complex with azide, Biophys. J. 104 (2013) 377–385.
[17] C. del Val, L. Bondar, A.-N. Bondar, Coupling between inter-helical hydrogen bonding and water dynamics in a proton transporter, J. Struct. Biol. 186 (2014) 95–111.
[18] M. Kubo, et al., Role of Arg123 in light-driven anion pump mechanisms of pharaonis Halorhodopsin, Photochem. Photobiol. 85 (2009) 547–555.
[19] J. Gullingsrud, J. Saam, J. Phillips, psfgen User's Guide version 1.6, 2012.
[20] B.R. Brooks, CHARMM: the biomolecular simulation program, J. Comput. Chem. 30 (2009) 1545–1614.
[21] A.D. MacKerell Jr., et al., All-atom empirical potential for molecular modeling and dynamics studies of proteins, J. Phys. Chem. B 102 (18) (1998) 3586–3616.
[22] J.B. Klauda, et al., Update of the CHARMM all-atom additive force field for lipids: validation on six lipid types, J. Phys. Chem. B 114 (2010) 7830–7843.
[23] W.L. Jorgensen, et al., Comparison of simple potential functions for simulating liquid water, J. Chem. Phys. 79 (2) (1983) 926–935.
[24] E. Tajkhorshid, et al., Molecular dynamics study of the nature and origin of retinal's twisted structure in bacteriorhodopsin, Biophys. J. 78 (2000) 683–693.
[25] M. Nina, B. Roux, J.C. Smith, Functional interactions in bacteriorhodopsin: a theoretical analysis of retinal hydrogen bonding with water, Biophys. J. 68 (1995) 25–39.
[26] J.C. Phillips, et al., Scalable molecular dynamics with NAMD, J. Comput. Chem. 26 (2005) 1781–1802.
[27] H. Grubmüller, et al., Generalized Verlet algorithm for efficient molecular dynamics simulations with long-range interactions, Mol. Simul. 6 (1991) 121–142.
[28] T. Darden, D. York, L. Pedersen, Particle mesh Ewald: An N•log(N) method for Ewald sums in large systems, J. Chem. Phys. 98 (1993) 10089–10092.
[29] U. Essmann, et al., A smooth particle mesh Ewald method, J. Chem. Phys. 103 (1995) 8577–8593.
[30] J.-P. Ryckaert, G. Ciccotti, H.J.C. Berendsen, Numerical integration of the Cartesian equations of motion of a system with constraints: Molecular dynamics of n-alkanes, J. Comput. Phys. 23 (1977) 327–341.
[31] S. Miyamoto, P. Kollman, An analytical version of the SHAKE and RATTLE algorithm for rigid water models, J. Comput. Chem. 13 (1992) 952–962.
[32] G.J. Martyna, D.J. Tobias, M.L. Klein, Constant-pressure molecular-dynamics algorithms, J. Chem. Phys. 101 (1994) 4177–4189.
[33] S.E. Feller, et al., Constant pressure molecular dynamics simulation: the Langevin piston method, J. Chem. Phys. 103 (11) (1995) 4613–4621.
[34] W. Humphrey, W. Dalke, K. Schulten, VMD: visual molecular dynamics, J. Mol. Graph. 14 (1) (1996) 33–38.
[35] A. Sali, T.L. Blundell, Comparative protein modelling by satisfaction of spatial restraints, J. Mol. Biol. 234 (1993) 779–815.
[36] N. Eswar, et al., Tools for comparative protein structure modeling and analysis, Nucleic Acids Res. 31 (2003) 3375–3380.
[37] A. Aksimentiev, K. Schulten, Imaging alpha-hemolysin with molecular dynamics: Ionic conductance, osmotic permeability and the electrostatic potential map, Biophys. J. 88 (88) (2005) 3745–3761.
[38] Y. Furutani, et al., Dynamics of dangling bonds of water molecules in pharaonis halorhodopsin during chloride ion transportation, J. Phys. Chem. Lett. 3 (2012) 2964–2969.
[39] C. del Val, S.H. White, A.-N. Bondar, Ser/Thr motifs in transmembrane proteins: conservation patterns and effects on local protein structure and dynamics, J. Membr. Biol. 245 (2012) 717–730.
[40] H. Jayaram, et al., Structure of a slow CLC Cl^-/H^+ antiporter from a cyanobacterium, Biochemistry 50 (2011) 788–794.
[41] R.E. Hibbs, E. Gouaux, Principles of activation and permeation in an anion-selective Cys-loop receptor, Nature 474 (2011) 54–60.
[42] H. Ohtaki, T. Radnai, Structure and dynamics of hydrated ions, Chem. Rev. 93 (1993) 1157–1204.
[43] A. Gruia, et al., Mechanism of a molecular valve in the halorhodopsin chloride pump, Structure 13 (2005) 617–627.
[44] M.A. Seeger, et al., Structural asymmetry of AcrB trimer suggests a peristaltic pump mechanism, Science 313 (2006) 1295–1298.
[45] G.B. Erkens, et al., Unsynchronised subunit motion in single trimeric sodium-coupled aspartate transporters, Nature 502 (2013) 119–123.
[46] E.R. Georgieva, et al., Conformational ensemble of the sodium-coupled aspartate transporter, Nat. Struct. Mol. Biol. 20 (2013) 215–221.
[47] Z. Cao, J.U. Bowie, Shifting hydrogen bonds may produce flexible transmembrane helices, Proc. Natl. Acad. Sci. U. S. A. 109 (21) (2012) 8121–8126.
[48] A.-N. Bondar, S.H. White, Hydrogen bond dynamics in membrane protein function, Biochim. Biophys. Acta 1818 (2012) 942–950.
[49] J. Otomo, Anion selectivity and pumping mechanism of halorhodopsin, Biophys. Chem. 56 (1995) 137–141.
[50] M. Shibata, et al., Deprotonation of Glu234 during the photocycle *of Natronomonas pharaonis* halorhodopsin, Chem. Phys. Lett. 432 (2006) 545–547.
[51] M. Sato, et al., Ser-130 of *Natronobacterium pharaonis* halorhodopsin is important for the chloride binding, Biophys. Chem. 104 (2003) 209–216.